Microstructured barbs on the North American porcupine quill enable easy tissue penetration and difficult removal

Woo Kyung Cho[a,b,c], James A. Ankrum[a,b], Dagang Guo[a,d], Shawn A. Chester[e], Seung Yun Yang[a,b,f], Anurag Kashyap[a], Georgina A. Campbell[a,g], Robert J. Wood[h], Ram K. Rijal[a], Rohit Karnik[e], Robert Langer[b,c,i,1], and Jeffrey M. Karp[a,b,f,1]

[a]Division of Biomedical Engineering, Department of Medicine, Center for Regenerative Therapeutics, Brigham and Women's Hospital, Harvard Medical School, Boston, MA 02115; [b]Harvard-MIT Division of Health Sciences and Technology, Massachusetts Institute of Technology, Cambridge, MA 02139; [c]David H. Koch Institute for Integrative Cancer Research, Massachusetts Institute of Technology, Cambridge, MA 02139; [d]Center for Biomaterials and Nano-Coating Research, State Key Laboratory for Mechanical Behavior of Materials, School of Material Science and Engineering, Xi´an Jiaotong University, Xi´an City, Shannxi Providence, 710049, China; [e]Department of Mechanical Engineering, Massachusetts Institute of Technology, Cambridge, MA 02139; [f]Harvard Stem Cell Institute, Cambridge, MA 02138; [g]Department of Material Engineering, Trinity College, Oxford OX1 3BH, United Kingdom; [h]School of Engineering and Applied Sciences, Harvard University, Cambridge, MA 02138; and [i]Department of Chemical Engineering, Massachusetts Institute of Technology, Cambridge, MA 02139

Edited by David A. Weitz, Harvard University, Cambridge, MA, and approved November 2, 2012 (received for review September 20, 2012)

North American porcupines are well known for their specialized hairs, or quills that feature microscopic backward-facing deployable barbs that are used in self-defense. Herein we show that the natural quill's geometry enables easy penetration and high tissue adhesion where the barbs specifically contribute to adhesion and unexpectedly, dramatically reduce the force required to penetrate tissue. Reduced penetration force is achieved by topography that appears to create stress concentrations along regions of the quill where the cross sectional diameter grows rapidly, facilitating cutting of the tissue. Barbs located near the first geometrical transition zone exhibit the most substantial impact on minimizing the force required for penetration. Barbs at the tip of the quill independently exhibit the greatest impact on tissue adhesion force and the cooperation between barbs in the 0–2 mm and 2–4 mm regions appears critical to enhance tissue adhesion force. The dual functions of barbs were reproduced with replica molded synthetic polyurethane quills. These findings should serve as the basis for the development of bio-inspired devices such as tissue adhesives or needles, trocars, and vascular tunnelers where minimizing the penetration force is important to prevent collateral damage.

biomimicry | medical tape | microneedle | sutures | staples

The North American porcupine has ~30,000 quills on the dorsal surface (1) that are released when a predator contacts the porcupine. In contrast to other mammals such as the African porcupine, hedgehog, and echidna that have smooth spines, each quill tip contains microscopic backward facing barbs (1–4). It has been well documented that it is difficult to remove porcupine quills once the quills are lodged within tissue (typically through both skin and muscle) (1, 3). However, the forces involved in penetration and pull-out have yet to be described and a comprehensive mechanism remains elusive.

Results and Discussion

North American porcupine quills (Fig. 1*A*) have two distinct regions. The conical black tip contains a layer of microscopic backward facing barbs on its surface (Fig. 1*B*), whereas the cylindrical white base contains smooth scale-like structures (Fig. 1*C*). As shown in Fig. 1*D*, barbs overlap slightly and have dimensions ranging from 100 to 120 μm in length, with a maximum width of 35–45 μm. There is 1- to 5-μm space between the tip of each barb and the shaft of the quill. The size of the barbs becomes larger farther from the apex of the tip (Fig. 1*E*). Because the length of the barbed region varies (Fig. S1), we standardized tests by only using quills with a barbed region of 4 mm.

Fig. 1*F* shows the results of penetration–retraction tests including a barbless control quill whose barbs were carefully removed by gentle sanding to avoid altering the diameter of quill (Fig. S2). The force required for penetration into tissue was defined as the *penetration force* and the maximum force required to remove the quill with respect to baseline was defined as *pull-out force*. Surprisingly, Fig. 1*F* shows that the quill with barbs required 54% less penetration force compared with the barbless quill. Regarding pull-out force, quills with and without barbs required 0.44 ± 0.06 N and 0.11 ± 0.02 N, respectively, and the barbed quill required less work of penetration and higher work of removal (Fig. 1*G*). Also, the barbed quill requires significantly less force and work to penetrate into tissue, compared with an 18 gauge hypodermic needle, which has a diameter of 1.161 ± 0.114 mm, similar to the diameter of a porcupine quill (1.262 ± 0.003 mm) (Fig. 1*G*).

As an additional control for the presence of barbs, we performed penetration–retraction tests using the naturally barbless African porcupine quills (Fig. 1*F*). The work of penetration and work of removal were 2.13 ± 0.04 mJ and 0.22 ± 0.06 mJ, respectively (Fig. 1 *F* and *G*). The profile of the force versus extension plot for the African quill exhibited a similar profile to the barbless North American quill. Thus, barbs appear essential for both reducing penetration force and generating tissue adhesion.

During the penetration process, tissue initially deforms under the advancing quill tip until a critical load leads to tissue puncture (5, 6). At the critical load, the quill tip initiates a crack that expands the hole circumferentially through stretching and tearing tissue fibers, permitting the quill to penetrate into tissue. The rupture of the tissue surface occurs via a planar mode I crack ahead of the tip, and the crack faces are wedged open by the advancing quill similar to what has been described for needles (7, 8). The work of penetration is the energy absorbed by the tissue during the penetration process and includes the energy required to deform and tear the tissue upon penetration (9). The barbed quill requires less work of penetration (Fig. 1*G*) while minimizing tissue damage. Stress concentrations generated by the barbs during penetration likely stretches or tears tissue fibers locally at the interface of the quill.

To visualize the effect of barbs on penetration, we examined the strain distribution in tissue using finite element analysis (FEA) for

Author contributions: W.K.C., J.A.A., R.L., and J.M.K. designed research; W.K.C., J.A.A., D.G., S.A.C., S.Y.Y., A.K., G.A.C., and R.K.R. performed research; W.K.C., J.A.A., D.G., S.A.C., S.Y.Y., R.J.W., R.K., and J.M.K. analyzed data; and W.K.C., J.A.A., S.A.C., R.K., R.L., and J.M.K. wrote the paper.

The authors declare no conflict of interest.

This article is a PNAS Direct Submission.

[1]To whom correspondence may be addressed. E-mail: jkarp@rics.bwh.harvard.edu or rlanger@mit.edu.

This article contains supporting information online at www.pnas.org/lookup/suppl/doi:10.1073/pnas.1216441109/-/DCSupplemental.

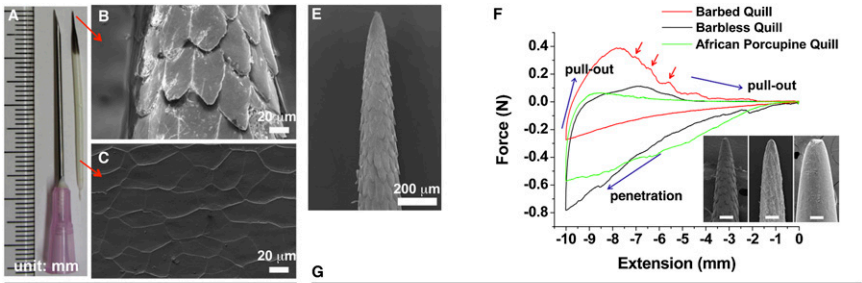

G

	Penetration Force (N)	Pull-out Force (N)	Work of Penetration (mJ)	Work of Removal (mJ)
Barbed Quill	0.33 ± 0.08	0.44 ± 0.06	1.08 ± 0.37	1.73 ± 0.41
Barbless Quill	0.71 ± 0.09*	0.11 ± 0.02*	2.41 ± 0.28*	0.28 ± 0.03*
18 Gauge Needle	0.59 ± 0.11*	0.04 ± 0.006*†	2.75 ± 0.70*	0.10 ± 0.02*
African Porcupine Quill	0.65 ± 0.03*	0.06 ± 0.01*	2.13 ± 0.04*	0.22 ± 0.06*

Fig. 1. Geometrical features of the North American porcupine quill and analysis of the penetration and removal forces with muscle tissue. (*A*) North American porcupine quill. (*B* and *C*) FE-SEM images showing the microstructure of the quill tip and base, respectively. (*D*) Fluorescence image enables visual delineation of the geometry of single barbs. (*E*) FE-SEM image showing the microstructure of the tip of the porcupine quill. (*F*) Representative force versus extension plots show puncture, penetration, and removal of barbed, barbless, and African porcupine quills from muscle tissue (see Fig. S3*A* for experimental set-up). (*Inset*) Micron-level topography of the three quills. (Scale bars: 100 μm.) Red arrows indicate resistance as the barbed quill is removed from the tissue (not observed for others). (*G*) Summary of experimental values obtained from penetration/removal of barbed quill, barbless quill, 18 gauge needle, and African porcupine quill (mean ± SD, $n = 5$). Each mean is compared with every other mean using one-way ANOVA with Tukey's Honestly Significant Difference post hoc analysis to correct multiple comparisons at 95% confidence interval by using GraphPad Prism 6 (*$P < 0.05$, compared with barbed quill; †$P < 0.05$, compared with barbless quill).

a barbless quill and a simplified two-barbed quill (Fig. S4 *A* and *B*). Values for the geometry and material properties of the quill and tissue for FEA were experimentally derived (Fig. S4*C*). The analysis revealed that tissue is primarily stretched and deformed by high stress concentrations near the barbs. The local stress concentrations likely reduce the need to deform the entire circumference of tissue surrounding the quill, consequently reducing the penetration force. The concept of stress concentration has been used to design blades and knives, albeit at a much larger scale than what is used by porcupine quills. Compared with straight blades, serrated blades require less work to cut tissue by localizing strain at points on the tips of the teeth of the blade. The strain concentration causes the tissue to fail with a lower input force (10). Consequently, serrated blades provide cleaner cuts with minimal deformation of the tissue (10).

Although porcupine quill barbs are relatively small compared with the jagged edge of a serrated knife, we observed a cleaner interface between tissue and barbed quills compared with barbless quills upon histological analysis of the tract left by quills after penetration (Fig. 2 *A* and *B*). This result suggests that the tissue absorbs less energy and is damaged less during penetration by a barbed quill. Furthermore, when 0.2 N was applied to barbed and barbless quills, the barbed quills advanced significantly deeper into muscle (4.19 ± 0.39 mm) than barbless quills (2.50 ± 0.33 mm) (Fig. 2 *C*–*E*) as measured by microcomputed tomography (micro-CT).

To investigate the role of barb deflection in the reduction of penetration force, we reproduced quills with nondeployable barbs using replica molding that reproduces the surface topography of the quill. We fabricated both barbless and barbed (nondeployable) polyurethane (PU) quills by replica molding (Fig. 3 *A* and *B*). Although the penetration force for insertion of barbless PU quills to a depth of 4 mm was 0.046 ± 0.010 N, the barbed PU quill required 35% less force, 0.030 ± 0.006 N (Fig. 3*C*). Additionally, the penetration force of natural barbed quills with muscle tissue was 0.043 ± 0.013 N (Fig. 3*D*), which was not significantly different from that of the PU barbed quill. Although the barbs of the PU quill cannot bend, the PU quill includes the same topography (i.e., barbs) creating stress concentrations during penetration into the tissue. Therefore, the experimental results with the fabricated PU quills support that stress concentration at barbs helps to reduce the penetration force of the natural porcupine quill. As barbs and muscle tissue fibers are on the same length scale (~50–100 μm) (11), the stress concentrations at barbs can potentially stretch tissue fibers locally. To apply this phenomenon to the development of a medical needle to achieve reduced penetration force (see *SI Text*), we fabricated a prototypic hypodermic needle with

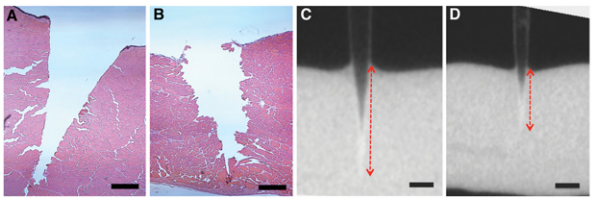

E

	Penetrating Depth (mm) after 0.2N Applied Force
Barbed Quill	4.19 ± 0.39
Barbless Quill	2.50 ± 0.33

Fig. 2. Barbs reduce tissue damage and facilitate penetration into tissue. (*A, B*) Representative histological images of tissue samples that were penetrated with barbed and barbless quills, respectively, showing significantly less damage induced by the barbed quills ($n = 5$). (Scale bar: 200 μm.) (*C* and *D*) Microcomputed tomography (Micro-CT) images present the penetrated barbed (*C*) and barbless (*D*) quills within tissue. Both quills were penetrated into tissue with an applied force of 0.2 N. The red dashed arrows indicate the penetrating depth of quill. (Scale bar: 1 mm.) (*E*) Mean penetrating depth of barbed and barbless quills observed in micro-CT images ($n = 3$).

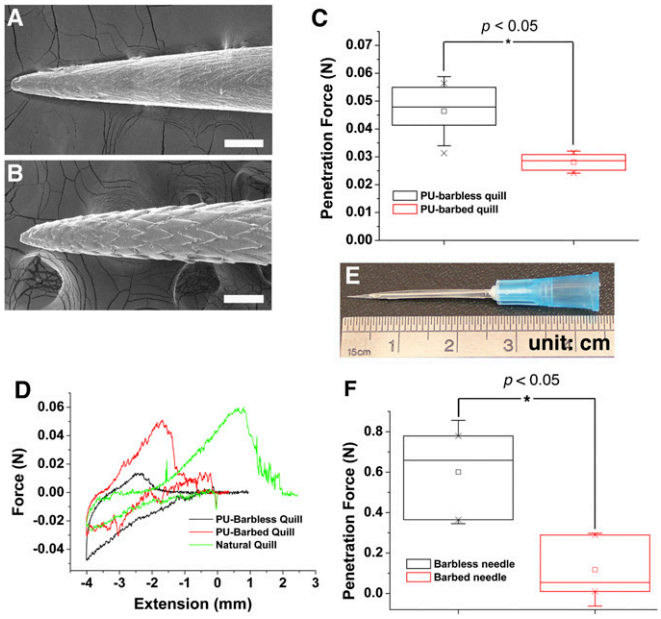

Fig. 3. The reduced penetration force of the natural porcupine quill can be replicated in synthetic polyurethane quills. (*A* and *B*) FE-SEM images show the barbless and barbed synthetic PU quills. (Scale bar: 100 μm.) (*C*) The forces required to penetrate the PU quills into muscle tissue to 4 mm-depth (see Fig. S3*B* for experimental details). The mean values are shown with SD (n = 5, Student t test at the level of 95% significance). The box plot whiskers are set to ±1.2 SD. (*D*) Representative force versus extension plots from the penetration–retraction tests of the natural quill and replica molded PU quills performed in muscle tissue. (*E*) Fabricated quill-mimetic needle. (*F*) The forces required to penetrate the fabricated barbed/barbless needles into a model of human skin. The data shows the mean penetration force with SD (n = 3, each needle was used at least four times, Student t test at the level of 95% significance). The two "X"s in box plots of *C* and *F* indicate first and 99th percentiles.

microscopic barbs. The PU-barbed needle showed 80% less penetration force compared with the PU barbless needle (Fig. 3 *E* and *F*).

Upon penetration of a quill into tissue, tensile and compressive "zones" arise in the surrounding tissue. The quill has three geometrical transition zones as shown in Fig. 4*A*. FEA shows that tissue compression occurs tangential to the quill from the first transition zone, which is ∼3 mm from the apex of tip with a maximum at the second transition zone (Fig. S4*D*). This suggests that barbs closest to the first transition zone may experience the greatest interaction with tissue. To understand the interaction and contribution of each region of the barbed tip, we isolated individual regions of quill tips via sanding (Fig. S5). Compared with the barbless quill, the penetration force does not decrease if only the first 1 or 2 mm of barbed region at the tip of the quill is included (quills 3 and 4). However, when barbs in the 2–3 mm region are included, the penetration force significantly decreases. Quill 6, which has barbs only in the 2–4 mm region, resulted in a significant reduction of penetration force, ∼0.26 N. Additionally, the 2–3 mm (quill 7) and 3–4 mm (quill 8) barbed regions independently reduce the penetration force compared with the barbless quill (quill 1). Therefore, it appears the 2–4 mm barbed region close to the first transition zone is most critical for reducing the penetration force.

The presence of barbs contributes 0.33 N of pull-out force (comparing quills with a 4 mm barbed region to barbless quills; $\Delta_{12} = 0.33$). The 1–3 mm barbed region had less impact on pull-out force compared with the 1 mm region at the tip (Comparing quill 3 with 5). Comparing the pull-out forces between quill 5 and 2 ($\Delta_{52} = 0.14$) suggests that the 1 mm region near the transition zone (at the base) is likely critical. However, the presence of barbs solely in the 2–4 mm region (quill 6) or in the 2–3 mm region (quill 7) did not substantially increase pull-out force compared with the barbless quill. Furthermore, barbs in the 3–4 mm region alone did not increase the pull-out force. This data suggests that barbs in different regions likely work cooperatively. Cooperativity is further supported by the lack of additive effects ($\Delta_{14} + \Delta_{16} \neq \Delta_{12}$ and $\Delta_{15} + \Delta_{18} \neq \Delta_{12}$). Taken together, the first 1 mm barbed region of tip independently makes the greatest impact on pull-out force, and the cooperation between 0–2 mm and 2–4 mm regions increases the force. Cooperativity may be a function of barb overlap where increased compressive force from tissue on barbs near the transition zone impacts barbs closer to the tip. Or barbs near the tip may experience different stresses due to the cutting of tissue by the more proximal barbs. Fig. 4*D* shows the summary of work of removal for all quill preparations. Together, these data suggest that the quill achieves adhesion by a mechanism that is more complex than simply hooking tissue fibers.

To examine how barbs generate mechanical adhesion, we investigated quill removal from both fibrous tissue and a nonfibrous control (Fig. S6 and *SI Text*). Tissue fibers interlock under the barbs, suggesting barbs may be deployed or bent during removal from tissue. We postulated that such deployment of the barbs could increase tissue adhesion by projecting barbs radially away from the quill (thus increasing the apparent quill diameter) to significantly increase frictional resistance and promote further mechanical interlocking with tissue. The ability of deployment or bending of barbs to contribute to tissue adhesion was further tested with porcine skin, which has similar mechanical properties to human skin (12, 13). The deployment or bending of barbs was observed following penetration–retraction tests with significant residual tissue adhered to the quill (Fig. 5 *A*–*D*). The pull-out force for porcine skin was 2.36 ± 0.83 N (Fig. 5*E*), whereas the work of removal was 2.34 ± 0.68 mJ. Interestingly, we observed a direct correlation between the pull-out force and the number of bent barbs following removal of the quill from skin (Fig. 5 *F*–*I*) and significantly greater work is required to remove a natural quill from muscle tissue compared with a PU barbed quill (Fig. 3*D*). Natural quill with deployable barbs requires 0.144 ± 0.048 mJ for removal, compared with 0.053 ± 0.023 mJ for nondeployable PU-barbed quill. The PU-barbed quill produces the maximum force after 2 mm of pull-out and then disengages the tissue completely at 4 mm of pull-out. However, natural quill drags tissue for a relatively long displacement generating peak-adhesion after it has been pulled beyond 4 mm. The natural quill is able to stretch tissue maximally during removal by using the bending of barbs, which increases engagement with tissue fibers. The nondeployable barbs of the PU quill, however, pull tissue and cut as the quill is removed.

Reproducing the strong tissue adhesion property of the porcupine quill would be useful for the development of mechanically interlocking tissue adhesives. As a proof of concept, we fabricated a prototypic quill-mimetic patch that has a hexagonal array of 7 replica molded PU quills (Fig. 6*A*). Although the barbless PU quill patch showed minimal pull-out resistance (0.063 ± 0.033 N), the barbed PU quill patch achieved significantly greater tissue adhesion (0.219 ± 0.059 N, Fig. 6*B*). The work of removal for the barbed quill patch was >30× that of the barbless quill patch (Fig. 6*B*). As observed in Fig. 6*C*, the barbed quill array achieved significant interlocking with tissue whereas the barbless quill array achieved minimal interaction with tissue and thus could be easily removed. Although current barbed array systems have shown tissue adhesion, all of them feature initially deployed barbs that require high penetration force and cause tissue damage during penetration (14, 15). The quill-mimetic patch is unique in that it can both easily penetrate tissue and achieve high tissue adhesion.

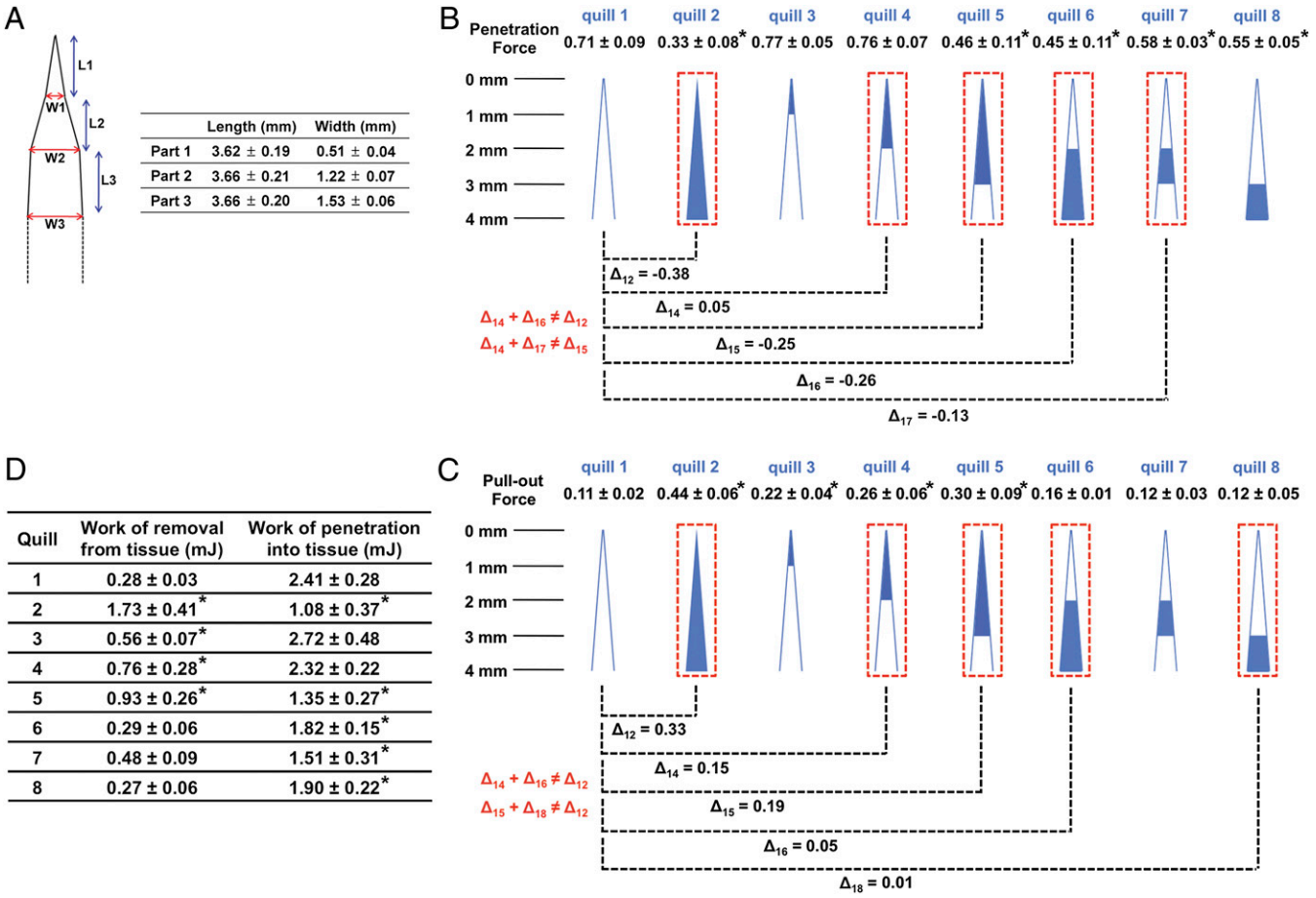

Fig. 4. Barbs within a 4-mm barbed region at the apex of the quill work independently to minimize penetration force and cooperatively to maximize pull-out from tissue. (*A*) Dimensional analysis of the porcupine quill through length scale measurements of natural quills (mean ± SD, $n = 5$). In terms of curvature, there are three transition points. L and W indicate length and width, respectively. (*B, C*) Penetration and pull-out forces were obtained with the prepared quills via sanding to isolate the contribution of barbs within different regions (see Fig. S5) (mean ± SD, $n = 5$). The penetrating depth for all experiments was 10 mm (see Fig. S3*A* for the experimental set-up). Cartoons depict quills prepared with specific lengths of barbs obtained through ablation with sand paper. The blue color indicates the barbed region and the white color indicates the barbless region. The penetration and pull-out forces of the prepared quills are compared with those of the barbless quill (quill 1). The difference in force is defined as Δ_{ij} (Δ_{ij} = penetration (or pull-out) force of *quill j*–penetration (or pull-out) force of *quill i*)). (*D*) Summarized work of penetration and work of removal obtained through penetration–retraction tests with muscle tissue (mean ± SD, $n = 5$). All are compared with quill 1 (*$P < 0.05$, one-way ANOVA Fisher's Least Significant Difference post hoc analysis at 95% confidence interval by using GraphPad Prism 6).

Conclusions

Herein we report how the North American porcupine quill displays a unique geometry that serves two polar opposite functions. Barbs on quills enable easy penetration into tissue and strong tissue adhesion during removal through the presence of backward facing deployable barbs. Similar to how biomimicry of cockleburs inspired the development of Velcro hook-and-loop fastener (16) and gecko is inspiring the development of tape-based tissue adhesives (17, 18), these findings should serve as the basis for the bio-inspired development of new devices including needles for easy penetration with compliant substrates such as tissue or microneedles where effective insertion without deformation (buckling) is required (19). Mimicking the porcupine quill should be useful for biomedical applications including local anesthesia, abscess drainage, vascular tunneling, and trocar placement in addition to the development of mechanically interlocking tissue adhesives.

Materials and Methods

Materials. North American (specifically, Pacific Northwest) porcupine quills and African porcupine quills were purchased from Minute Bear Trading. Fluorescein (sodium salt, dye content ~70%, Aldrich), rhodamine B (dye content ~90%, Sigma-Aldrich), ethanol (ACS reagent, ≥ 99.5%, 200 proof, Sigma-Aldrich), formalin solution [neutral buffered, 10% (vol/vol), Sigma], Sylgard 184 silicone elastomer kit (Dow Corning), UV-curable polyurethane acrylate (Minuta Technology), Irgacure 2959 (Ciba Specialty Chemicals), 18 gauge, 19 gauge, and 25 gauge needles (Becton Dickinson), artificial human skin (SynDaver Labs), muscle tissue of domesticated fowl (Shaw's), gelatin powder (DifcoTM, BD), sand paper (3M wetordry sandpaper 413Q 400 and Norton MultiSandTM, 60), cyanoacrylate glue (Loctite 495, Loctite), industrial razor blades (surgical carbon steel, single edged No. 9, VWR), polyether ether ketone (PEEK) hex nuts (Small Parts), silicone rubber film with backing adhesive (McMaster-Carr), pin mount stubs (25.4 mm in diameter, 9.5 mm in height, and 3.2 mm in pin diameter, Ted Pella), 5 min and 60 min epoxy glues (ITW Performance Polymers) were used as received. The fresh porcine skin was purchased from a local butcher shop.

Penetration–Retraction Tests with Muscle Tissue and Gelatin Gel. Penetration–retraction tests were performed with the mechanical tester (Model 5540, Instron). Only quills with a barbed region of 4 mm in length were selected for testing, as measured with a millimeter ruler and a dissecting optical microscope (SZ-6 PLUS, Cambridge Instruments). The muscle tissue was cut into specimens with 3–4 cm width, 2–3 cm length, and 4–5 mm thickness using a razor blade. The tissue specimens were mounted within the lower grips at the base of the mechanical tester. During fixation, care was taken not to excessively compress the tissue. After the specimen was fixed

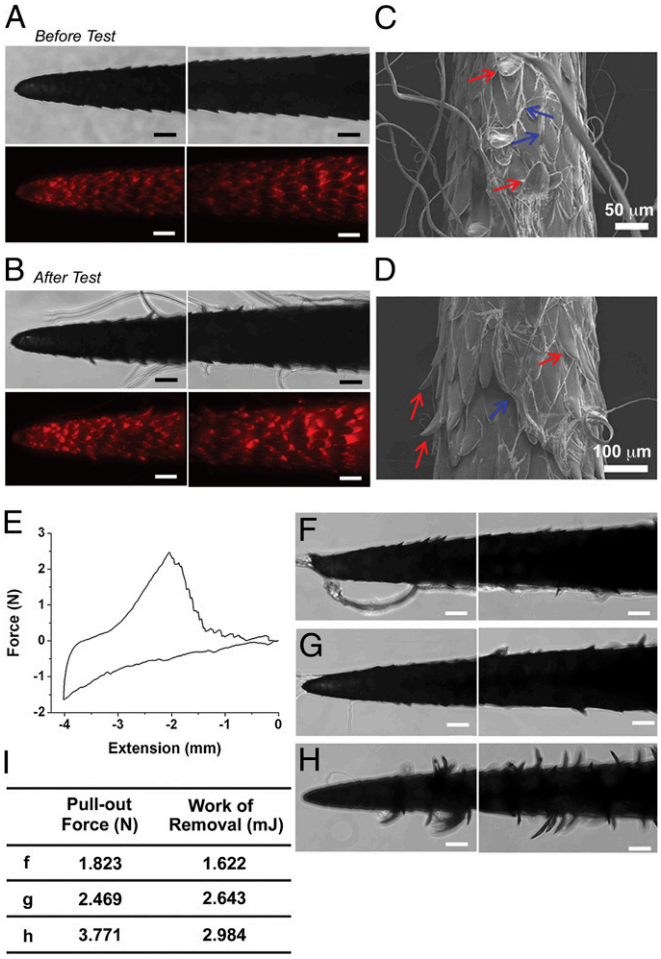

I

	Pull-out Force (N)	Work of Removal (mJ)
f	1.823	1.622
g	2.469	2.643
h	3.771	2.984

Fig. 5. Generation of mechanical adhesion by microstructured barbs. (*A* and *B*) Representative optical and fluorescent images of porcupine quills before and after removal from porcine skin. Fluorescence images are useful to delineate the boundaries of individual barbs and are obtained by merging several images taken at different focal planes along the *z* axis. (Scale bar: 100 μm.) (*C* and *D*) FE-SEM micrographs following removal of quills from porcine skin. Residual tissue is indicated by blue arrows. Red arrows in figures indicate bending of barbs during pull-out. (*E*) A representative force versus extension plot for a penetrating depth of 4 mm where puncture typically occurs following tissue compression of 1–2 mm ($n = 5$). (*F–H*) Images of quills following removal from porcine skin are useful to examine the heterogeneity of tissue interactions and to establish the relationship between the bending of barbs and relative level of tissue adhesion summarized in the table (*I*). (Scale bars: 100 μm.) See Fig. S3*A* for the experimental set-up for the tests with porcine skin.

between the grips, the exposed excess tissue over the grips was cut with a blade, generating a flat tissue surface (Fig. S3*A*). The explanted muscle tissue was static, aside from when it was compressed during penetration followed by elastic relaxation as insertion force was removed. The quill was fixed between the upper grips and the tip adjusted to contact the tissue surface. The quill was penetrated into the muscle tissue to the desired depth, typically 10 mm, at a rate of 1 mm/s and was pulled out at a rate of 0.033 mm/s to study how the barbs function during removal from tissue. For the duration of all experiments, the tissue was kept moist with PBS. Each quill was used for a single measurement. For details of experiment with gelatin gel as a nonfibrous tissue control, please see *SI Text*.

Preparation of the Stained Quills for Visualization During Adhesive Measurements. Porcupine quills were immersed into 0.01% aqueous fluorescein or rhodamine B solution. After 1 h, quills were removed from the staining solution and washed thoroughly with water. The stained quills were dried overnight before use.

Penetration–Retraction Tests with Porcine Skin. Fresh porcine skin was cut into specimens with 3–4 cm width and 3 cm length using a razor blade. For adhesive measurements, porcupine quills were inserted into porcine skin, vertically aligned within the lower grips, with a penetrating depth of 4 mm. The remainder of the test followed the procedure previously described for muscle tissue.

Surface Characterization of the Quills. The microstructures of the porcupine quills before and after penetration–retraction tests were examined with field-emission scanning electron microscope (FE-SEM, JEOL 5910) following a 30 nm-thick gold sputter coating. Light and fluorescence images were obtained with a Nikon Eclipse TE-2000-U microscope (Nikon Digital Sight DS-QiMC camera). The length of barbed region of each quill was examined with a dissecting optical microscope (SZ-6 PLUS, Cambridge Instruments) and optical digital images were obtained (IXY Digital, Canon).

Histological Analysis. The porcupine quill was penetrated into muscle tissue at a rate of 1 mm/s until the force reached 0.2 N. The sample was then fixed by immersing it into 10% (vol/vol) neutral buffered formalin for 24 h. The fixed sample was washed with water and stored in 70% (vol/vol) ethanol before embedding in paraffin. The sample was then dehydrated with 95% (vol/vol) and 100% ethanol solutions and embedded in paraffin (Thermo Electron Shandon Excelsior tissue processor). Five-micrometer sections of embedded samples were obtained with a rotary microtome (Thermo Scientific Shandon Finesse ME+). Sections were stained with hematoxylin and eosin, coverslipped with a xylene-based mounting medium, and the prepared slides were examined with a Nikon Eclipse TE-2000-U microscope (Nikon Digital Sight DS-QiMC camera).

Micro-Computed Tomography (Micro-CT). The porcupine quill was penetrated into muscle tissue at a rate of 1 mm/s until the force reached 0.2 N. The sample was then fixed by immersing it into 10% (vol/vol) neutral buffered formalin for 24 h. The fixed sample was washed with water and dehydrated. For each 25% (vol/vol), 50% (vol/vol), 75% (vol/vol), and 100% ethanol solutions, the sample was incubated for 30 min. The sample was then evaluated using a microtomographic imaging system (eXplore CT 120, Gamma Medica). CT slices of the sample were acquired by using 1,200 views with 25-μm isotropic voxels, a tube voltage of 80 kVp, 32-mA current, and 100-ms exposure time. The sample images were obtained to include the entire region of the quill and tissue. Images were reconstructed, filtered, and a specimen-specific threshold was applied. The penetrating depth of the porcupine quill within tissue was computed by using a direct 3D approach that does not rely on assumptions regarding the underlying structure.

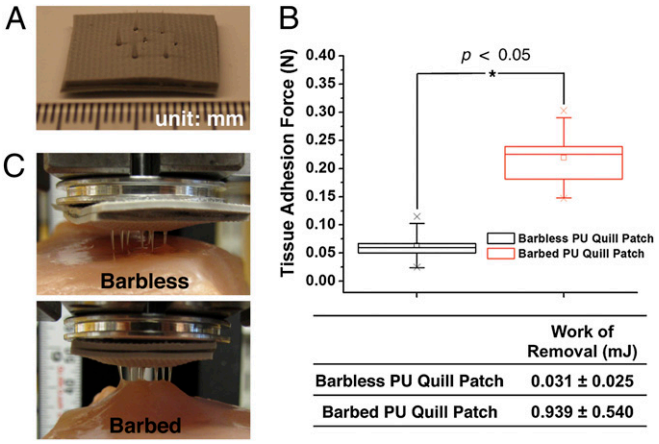

	Work of Removal (mJ)
Barbless PU Quill Patch	0.031 ± 0.025
Barbed PU Quill Patch	0.939 ± 0.540

Fig. 6. A prototypic quill-mimetic patch as a mechanically interlocking tissue adhesive. (*A*) The digital photograph shows the fabricated quill-mimetic patch, which consists of 7 PU barbless or barbed quills. (*B*) The tissue adhesion forces obtained from barbless and barbed PU quill patches ($n = 5$, Student *t* test at the level of 95% significance). The box plot whiskers are set to ±1.2 SD. The two "X"s in box plot indicate first and 99th percentiles. (*C*) Shows the quill-mimetic patches interacting with muscle tissue during the retraction process from muscle tissue.

Fabrication of Polyurethane Quills and Quill-Mimetic Needles. Poly(dimethylsiloxane) (PDMS) prepolymer was prepared by mixing the base material and curing agent in a 10:1 (wt/wt) ratio. After vigorous mixing and degassing, PDMS molds of natural barbed and barbless quills were prepared by thermal curing at 70 °C overnight. To make quill-mimetic needle, a 25 gauge needle was inserted into the quill's base. After curing PDMS, the quill and needle were removed to produce PDMS molds. The polyurethane acrylate, which was mixed with 0.1% photo-initiator, was added into the PDMS molds. To fabricate a quill-mimetic needle, a 25 gauge needle was again inserted into the mold at this stage allowing the polyurethane to bond to the needle. The samples were placed in a vacuum desiccator in the dark to degas the samples for 1–2 h. The samples were then cured under UV (254 nm) for 90 min and removed from the molds.

Measurement of Penetration Force of Polyurethane Quills and Needles with Tissue. A thick section of muscle tissue was prepared to fit with the available space between the lower grips of mechanical tester. The prepared tissue was placed between the grips without compression. The polyurethane (PU) quill was fixed between the upper grips of mechanical tester and the tip adjusted to contact the tissue surface. The quill was penetrated into the muscle tissue to the desired depth, 4 mm, at a rate of 1 mm/s. For the duration of all experiments, the tissue was kept moist with PBS. Each quill was used for a single measurement. The mean penetration force was measured from five different samples.

The penetration force of quill-mimetic PU needle was examined with artificial skin (SynDaver Labs) that mimics the property of human skin. The fabricated PU needle was connected with a force gauge (Model FGV-5XY, Nidec-Shimpo), and inserted manually into the skin. The force gauge reads the required penetration force. Each needle was used at least four times. The mean penetration force was obtained from three different samples.

Fabrication of a Quill-Mimetic Patch with a Hexagonal Array of PU Quills. The tip (5-mm length) of natural quills was replicated with a hex nut base and arranged in a hexagonal array with a silicone backing layer using 60 min epoxy glue. Following generation of PDMS molds of barbed or barbless quills, we followed the same procedure descried previously to produce replica molded PU quills. The 7-PU barbed/barbless samples were then assembled with silicone backing layer. The hex base of PU quills allowed for simple alignment of a hexagonal array. To ensure that the array was stable, another backing layer was attached to the assembled sample using 5-min epoxy glue. All PU quills within the patch were perpendicular to the backing layer.

Measurement of Tissue Adhesion Force of Quill-Mimetic Patch. A modification of ASTM F2258-05 was used to measure the tissue adhesion force of quill-mimetic patches. A flat section of muscle tissue was affixed using cyanoacrylate glue to a test fixture (i.e., pin mount stub with diameter of 25.4 mm). The prepared tissue sample was mounted within the lower grips at the base of the mechanical tester. The quill-mimetic patch was glued onto another fixture, and fixed between the upper grips of mechanical tester. The tips of quills within the patch were adjusted to contact the tissue surface. The patch was penetrated into the muscle tissue to a depth of 4 mm at a rate of 1 mm/s and was pulled out at a rate of 0.033 mm/s to study how the barbs function during removal from tissue. For the duration of all experiments, the tissue was kept moist with PBS. The mean tissue adhesion force was measured from five different samples.

Finite Element Analysis. For the finite element simulation, we used a 2D approximation of the geometry. We modeled the quill and barbs as a linear elastic material with Young's modulus $E = 3.25$ GPa and Poisson's ratio $\nu = 0.4$ as determined from uniaxial tension experiments of quill tips. The porcine skin is modeled as a nonlinear incompressible material using the inverse Langevin model (20, 21) with an initial shear modulus $\mu = 0.165$ MPa and locking stretch $\lambda_L = 1.81$. Please see the details in *SI Text*.

ACKNOWLEDGMENTS. We thank Dr. E. O'Cearbhaill and Bryan Laulicht for helpful discussions and Admet Inc. for generously providing an eXpert 760 mechanical tester that was instrumental for this work. This work was supported by National Institutes of Health (NIH) Grant GM086433 and American Heart Association Grant 0835601D (to J.M.K.); National Science Foundation Grant NIRT 0609182 and NIH Grant DE013023 (to R.L.); and National Research Foundation of Korea Grant NRF-2010-357-D00277 funded by the Korean Government (Ministry of Education, Science and Technology) (to W. K.C.). We thank the National Science Foundation Graduate Research Fellowship program and the Hugh Hampton Young Memorial Fund for supporting J. A.A., and the Massachusetts Institute of Technology Undergraduate Research Opportunities Program for supporting A.K. and R.K.R. We also thank the China Scholarship Council and the National Natural Science Foundation of China (no: 51273159; 51072159), Program for New Century Excellent Talents in Universities (Chinese Ministry of Education, 2301G107aaa, NCET-08-0444) for supporting D.G.

1. Roze U (2009) *The North American Porcupine* (Cornell Univ Press, Ithaca), 2nd Ed.
2. Vincent JFV, Owers P (1986) Mechanical design of hedgehog spines and porcupine quills. (Translated from English). *J Zool* 210:55–75.
3. Vaughan TA, Ryan JM, Czaplewski NJ (2000) *Mammalogy* (Saunders College Publishing, Philadelphia), 4th Ed.
4. Kurta A (1995) *Mammals of the Great Lakes Region* (Univ of Michigan Press, Ann Arbor) Revised Ed.
5. Azar T, Hayward V (2008) Estimation of the fracture toughness of soft tissue from needle insertion. *Biomedical Simulation, Proceedings*, eds Bello F, Edwards PJ, Lecture Notes in Computer Science (Springer, Berlin), Vol 5104, pp 166–175.
6. Shergold OA, Fleck NA (2005) Experimental investigation into the deep penetration of soft solids by sharp and blunt punches, with application to the piercing of skin. *J. Biomech. Eng Trans ASME* 127(5):838–848.
7. Shergold OA, Fleck NA (2004) Mechanisms of deep penetration of soft solids, with application to the injection and wounding of skin. *Proc R Soc London Ser A* 460(2050): 3037–3058.
8. Das S, Ghatak A (2011) Puncturing of soft gels with multi-tip needles. *J Mater Sci* 46(9):2895–2904.
9. Sharp AA, Ortega AM, Restrepo D, Curran-Everett D, Gall K (2009) In vivo penetration mechanics and mechanical properties of mouse brain tissue at micrometer scales. *IEEE Trans Biomed Eng* 56(1):45–53.
10. Anderson PSL, LaBarbera M (2008) Functional consequences of tooth design: Effects of blade shape on energetics of cutting. *J Exp Biol* 211(Pt 22):3619–3626.
11. Maier F, Bornemann A (1999) Comparison of the muscle fiber diameter and satellite cell frequency in human muscle biopsies. *Muscle Nerve* 22(5):578–583.
12. Ankersen J, Birkbeck AE, Thomson RD, Vanezis P (1999) Puncture resistance and tensile strength of skin simulants. *Proc Inst Mech Eng Part H-J Eng Med* 213(H6): 493–501.
13. Edwards C, Marks R (1995) Evaluation of biomechanical properties of human skin. *Clin Dermatol* 13(4):375–380.
14. Reed ML, Han H, Weiss LE (1992) Silicon micro-celcro. *Adv Mater (Deerfield Beach FL)* 4(1):48–51.
15. Griss P, Enoksson P, Stemme G (2002) Micromachined barbed spikes for mechanical chip attachment. *Sens Actuators A Phys* 95:94–99.
16. Forbes P (2006) *The Gecko's Foot: Bio-inspiration: Engineering New Materials from Nature* (W. W. Norton, New York).
17. Mahdavi A, et al. (2008) A biodegradable and biocompatible gecko-inspired tissue adhesive. *Proc Natl Acad Sci USA* 105(7):2307–2312.
18. Karp JM, Langer R (2011) MATERIALS SCIENCE Dry solution to a sticky problem. *Nature* 477(7362):42–43.
19. Yang M, Zahn JD (2004) Microneedle insertion force reduction using vibratory actuation. *Biomed Microdevices* 6(3):177–182.
20. Cohen A (1991) A pade approximant to the inverse Langevin function. *Rheol. Acta* 30(3):270–273.
21. Arruda EM, Boyce MC (1993) A three-dimensional constitutive model for the large stretch behavior of rubber elastic materials. *J Mech Phys Solids* 41(2):24.

Supporting Information

Cho et al. 10.1073/pnas.1216441109

SI Text

Potential to Mimic the Quill's Reduced Penetration Force. To harness the reduced penetration force of the quills in mimetic devices, we envision that barb-like features may be simply positioned on the tapered tip region of needles, trocars, or probes for several medical applications. The increased pull-out force due to the presence of barbs could lead to increased tissue damage during removal, however reduced penetration can be achieved with nondeployable barbs (such as those made from PU), which exhibit significantly reduced work of removal compared with natural quills (that likely tear more tissue during removal) (Fig. 3*D*). Furthermore, one could engineer degradable barbs or barbs that soften following penetration.

Barbs Produce Tissue Adhesion by Mechanically Interlocking with Tissue Fibers. To examine if mechanical interlocking through hooking tissue fibers contributes to the tissue-holding force, we performed penetration–retraction tests using gelatin gel as a model of a nonfibrous tissue. To match the gelatin gel density with that of muscle tissue, we initially determined the fibrous component of muscle tissue to be 0.237 ± 0.006 g/mL by obtaining the dry mass and wet volume (examined with a pycnometer) as previously described (1). Using the gelatin gel, we performed the tests with a penetrating depth of 4 mm. To prevent damage of the gelatin gel by gripping, the gel was placed on the mechanical tester without compression. This setup was repeated with muscle tissue accordingly to allow comparison of the gelatin and muscle data. As shown in Fig. S6*C*, the pull-out force generated with nonfibrous gelatin gel and a barbed quill was 0.009 ± 0.003 N which was significantly lower than the force required to remove the 4-mm-penetrated porcupine quill from fibrous muscle tissue, 0.052 ± 0.021 N. These data suggest that mechanical interlocking of tissue fibers by barbs is a significant factor to produce tissue adhesion.

SI Materials and Methods

Measurement of the Density of Muscle Tissue. Tissue density was measured using described methods (1). Briefly, the tissue density was determined using a 25 mL glass pycnometer with the following Eq. **S1**.

$$d_s = sd_w/(m_{pf} - m_t + s) \quad \textbf{[S1]}$$

where d_s is density of the tissue (g/mL), d_w is density of water (g/mL), s is weight of the dried tissue (g), m_{pf} is weight of pycnometer and water (g), and m_t is weight of pycnometer, water, and tissue. To obtain the weight of the dried tissue, the tissue had been dried in an oven at 60 °C until the weight plateaued after 7 d.

Alternative Experimental Set-up for Gelatin Gel and Muscle Tissue. The experiments with gelatin gel, used as a control for a nonfibrous tissue were performed with an alternative set-up, as gelatin gel could not be gripped. Compression stage instead of the lower grips was used to fix the gelatin gel during measurements. In other words, gelatin gel was fixed onto the stage without compression. Considering the different experimental set-up used with gelatin gel, we performed an additional test with muscle tissue by placing a thick section of tissue between lower grips without compression. To minimize any movement of muscle tissue, we prepared the chicken breast tissue that can fit with the available space between lower grips without compression (Fig. S3*B*). Gelatin gel was prepared with the same density as that of muscle tissue by dissolving gelatin powder into distilled water at 40 °C and letting it cool to room temperature. Quills that were removed from tissue/gelatin gel were examined to identify the potential of mechanical interlocking of tissue fibers by the microscopic barbs. Because the quill was consistently covered by tissue when 10 mm was used as the penetrating depth, thus obscuring observation of barbs, a penetrating depth of 4 mm was used. For the tissue and gelatin gel, the mean penetration force and mean pull-out force were measured from five different samples.

Measurement of the Young's Modulus and Tensile Strength of Porcupine Quill Tips for Finite Element Analysis Modeling. To accurately measure the Young's modulus of the tip, the top 1 mm near the apex was gripped with bottom grips leaving 2 mm exposed for measurement. We made the assumption that the cross-sectional diameter (~0.30 mm) of the exposed 2-mm-long region between the grips remained constant. Measurements were performed at a rate of 1 mm/min for five different samples.

Characterization of the Mechanical Properties of Porcine Skin for Finite Element Analysis Modeling. The specimen was cut into a dog bone shape (2 cm × 5 cm). To prevent the porcine skin from slipping from the grips, the porcine skin was covered with sand paper (grit number: P60) excluding the measured area. The sand paper was tightly affixed to the porcine skin using cyanoacrylate glue and staples. A uniaxial tensile test was performed to measure mechanical properties of the prepared porcine skin using an eXpert 760 mechanical tester (ADMET, Inc.). The rate for the tensile test was 1 mm/min and the obtained data were fitted using the inverse Langevin model of finite elasticity (2, 3).

Finite Element Analysis. For the finite element simulation of the two-barbed quill penetrating through skin, we used a 2D approximation of the geometry. The quill component consists of 946 Abaqus CPE3 triangular elements, and the tissue consists of 982 Abaqus CPE4H hybrid quadrilateral elements. We model the quill and barbs as a linear elastic material with Young's modulus $E = 3.25$ GPa and Poisson's ratio $\nu = 0.4$ as determined from uniaxial tension experiments of quill tips. To simulate the penetration of quills into the porcine skin, the mechanical response of porcine skin was analyzed and the tensile data were fitted to an inverse Langevin model for finite elasticity, and the rubbery modulus and network locking stretch of porcine skin was determined. The rubbery modulus of porcine skin was 0.05 ~ 0.28 MPa and its network locking stretch was 1.27 ~ 2.35. The failure strength of porcine skin was 8.2 ~ 15.4 MPa, which is similar to the values previously reported (4). For the finite element simulation, the skin is modeled as a nonlinear incompressible material using the inverse Langevin model (2, 3) with an initial shear modulus $\mu = 0.165$ MPa and locking stretch $\lambda_L = 1.81$. The simulation consists of two steps. To account for the already penetrated quill ahead of the section under consideration in this simulation, the quill is firstly translated to the right to prestress the tissue. Then in the second step, the quill is translated downward to slide across the tissue. This makes the model equivalent to considering a whole quill with only two barbs on its surface. Contact between the quill and the tissue is modeled with frictional coefficient of 0.1, which was used to model the penetration of medical needle into tissue (5).

For the finite element simulation of the barbless quill penetration into porcine skin, we used a 2D approximation of the geometry based on the properties of a natural quill (Fig. S4*D*). The mesh of the quill consists of 257 Abaqus CPE4R quadri-

lateral and 201 Abaqus CPE3 triangular elements, also the tissue consists of 17422 Abaqus CPE4H hybrid quadrilateral elements. The displacement boundary conditions that were imposed on the quill included symmetry along the left edge, whereas the top edge is given a downward displacement of 10 mm to penetrate the quill into the tissue. The displacement boundary conditions on the tissue included nodes along the bottom and right edges that are pinned, whereas the top edge is traction free. To model the "tearing" of the tissue due to the penetration of the quill, a cohesive interaction between the elements of the tissue along the left edge, and a rigid surface was defined. The cohesive interaction behaves elastically, with the same initial stiffness as the nonlinear elasticity in the tissue, and then fails (loses load carrying capacity) at a maximum normal stress of 10 MPa. We have modeled the geometry as plane-strain to maintain the "tearing" property of penetration, which enables variation of material parameters to observe the relative differences between simulations. In addition, a small gap would need to be introduced between the tissue and the axis of symmetry to permit the material to "open" for the quill to penetrate. The gap is needed not only to allow the quill to penetrate in the lack of cohesive elements, but also to keep the strains (and consequently stress) bounded because the hoop strain is the current distance to the centerline divided by the original distance to the centerline for a material point. For material points that lie on the centerline (or very near), the stresses quickly become very large. Contact between the quill and the tissue is modeled with a frictional coefficient of 0.1, which was used to model the penetration of a medical needle into tissue (5).

1. DiResta GR, et al. (1990) Measurement of brain tissue density using pycnometry. *Acta Neurochir Suppl (Wien)* 51:34–36.
2. Cohen A (1991) A pade approximant to the inverse Langevin function. *Rheol. Acta* 30(3):270–273.
3. Arruda EM, Boyce MC (1993) A three-dimensional constitutive model for the large stretch behavior of rubber elastic materials. *J Mech Phys Solids* 41(2):24.
4. Ankersen J, Birkbeck AE, Thomson RD, Vanezis P (1999) Puncture resistance and tensile strength of skin simulants. *Proc Inst Mech Eng Part H-J Eng Med* 213(H6):493–501.
5. Hauser K, Alterovitz R, Chentanez N, Okamura A, Goldberg K (2010) Feedback control for steering needles through 3D deformable tissue using helical paths. *Robotics: Sciences and Systems V*, eds. Trinkle J, Matsuoka Y, Castellanos JA (MIT Press, Cambridge), pp 37–44.

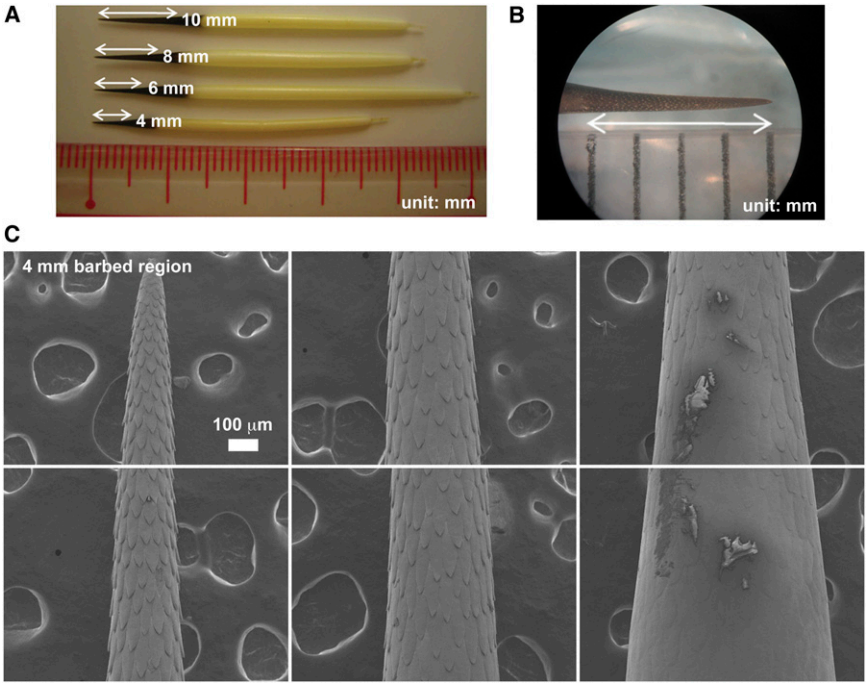

Fig. S1. Barbed regions vary between 4 and 10 mm in length. (*A*) Representative quills with different lengths of barbed regions where the length is typically in the range of 3–5 mm. (*B*) Optical microscopic image confirms the length of a quill with a 4-mm barbed region. (*C*) Sequential FE-SEM images of a single quill show the transition from functional barbs to a smooth surface containing barbs that have yet to emerge (i.e., those that cannot yet engage tissue).

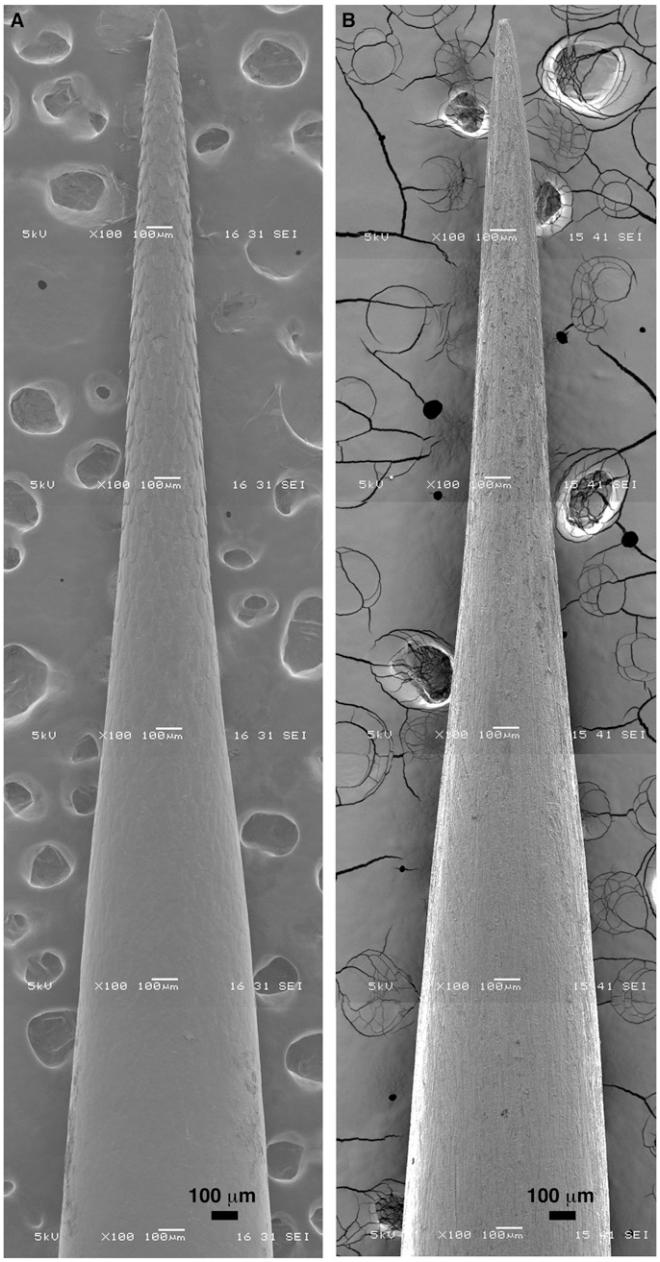

Fig. S2. Sanding of quills removes barbs but does not substantially alter the quill morphology or size. FE-SEM images show the barbed quill with 4 mm-barbed region (*A*) and the barbless quill after removal of the barbs by sanding (*B*). Gentle sanding didn't significantly change the diameter of quill. Specifically, whereas sanding of barbs led to a 3∼7% reduction in diameter for the first 0–2 mm from the apex of tip, sanding of other regions showed ∼1% reduction. *A* and *B* are composite images each formed by combining five sequential images.

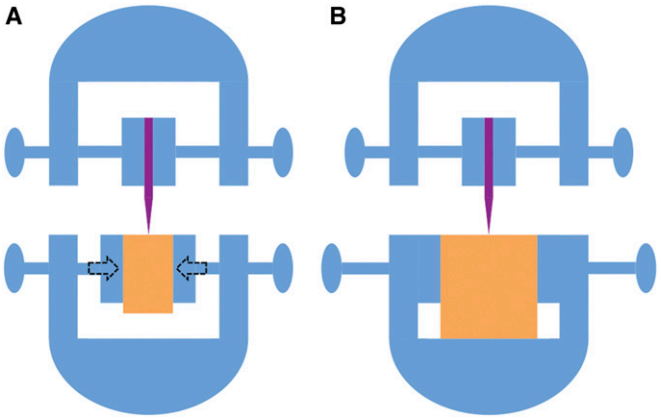

Fig. S3. Cartoon depicting the apparatus used for penetration–retraction tests. (*A*) Set-up for the test with muscle tissue, which was under compression. (*B*) Set-up for the test with muscle tissue without compression. The muscle tissue in *B* was cut to fit exactly with the available space within the lower platform. Purple and orange colors indicate the porcupine quill and muscle tissue, respectively. The set-up in *A* was used when we penetrated the porcupine quill into muscle tissue to a depth up to 10 mm. As the thickness of muscle tissue was <10 mm, we rotated the tissue vertically within the lower grips to allow penetration in the transverse direction. The set-up in *B* was used to adequately compare data from the tests with gelatin gel and muscle tissue. This comparison was useful to examine how barbs generate mechanical adhesion with tissue by examining quills following retrieval. To minimize any movement of muscle tissue, which was not under compression, we used thicker muscle tissue (i.e., chicken breast). Because the quill was consistently covered by tissue when 10 mm was used as a penetrating depth, obscuring observation of barbs, a penetrating depth of 4 mm was used. The penetrating depth of all tests with the set-up in *B* was 4 mm. The test with porcine skin was performed with the set-up in *A* because the skin was <10 mm thick. Furthermore, to study mechanisms of tissue adhesion with porcine skin, 4 mm was used as a penetrating depth. Note: we used the set-up in *A* for generating the data in Figs. 1, 4, and 5. We used the set-up in *B* for the data in Figs. 2, 3, and 6 and Fig. S6. It is important to consider that the differences in models impacted the force profiles and puncture and penetration forces. In the set-up in *A*, quill removal from tissue did not extend beyond zero in the force-extension curve. In the set-up in *B*, where tissue was not in compression (likely mimicking how quills penetrate tissue in nature), the quill is pulled beyond 0 when it is removed from tissue.

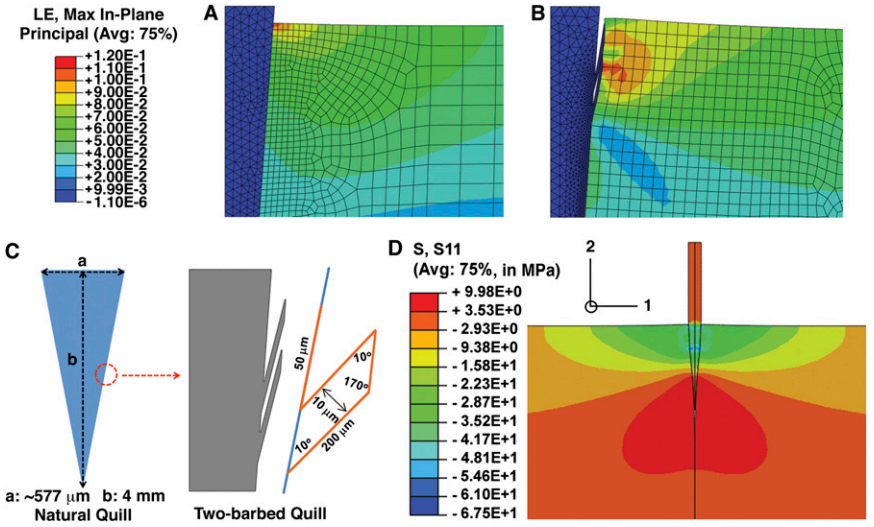

Fig. S4. Finite element analysis shows that the tissue is primarily stretched and deformed near the barbs. (*A* and *B*) Strain field distribution in skin tissue when a barbless quill or two-barbed is penetrated into tissue, respectively. The Young's modulus of both quills was set at 3.25 GPa for finite element analysis. LE refers to for Logarithmic (L) strain (ε) and represents true strain. 75% refers to the averaging threshold of the extrapolated results to achieve a smooth colored contour map. (*C*) Geometry of two-barbed quill with the dimensions of a single barb and the distance between two barbs indicated. The simplified geometry is based on the middle point of 4 mm barbed region of natural quill. (*D*) Finite element modeling of the quill penetration into skin tissue shows compressive stresses (in MPa) from the tissue acting on the quill at a distance from the quill tip. This is the stress state following a 10 mm-penetration into the skin tissue. S means stress and S11 refers to the stress vector on the plane normal to "1" in the "1" direction; 75% refers to the averaging threshold of the extrapolated results to achieve a smooth colored contour map.

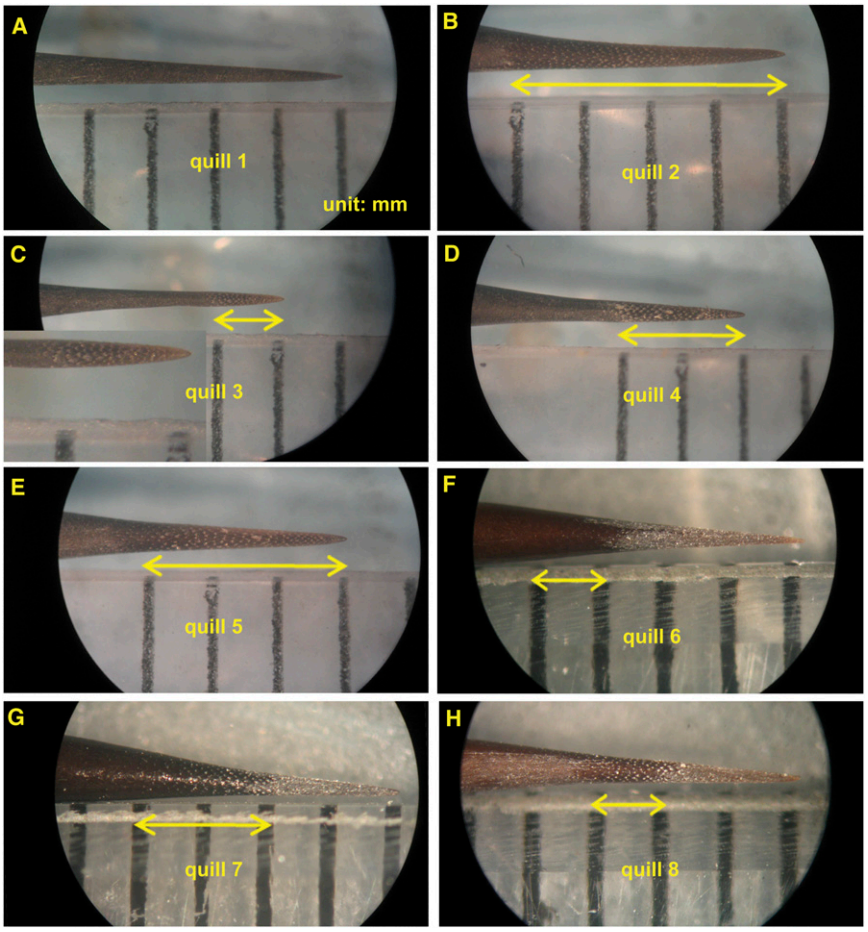

Fig. S5. Selective ablation of barbs is achieved by gentle sanding. (*A*–*H*) Representative optical micrographic images confirm the barbed region for eight quills that have been sanded to obtain barbed regions of specific length. *Inset* in *C* shows the enlarged image for 1-mm barbed region.

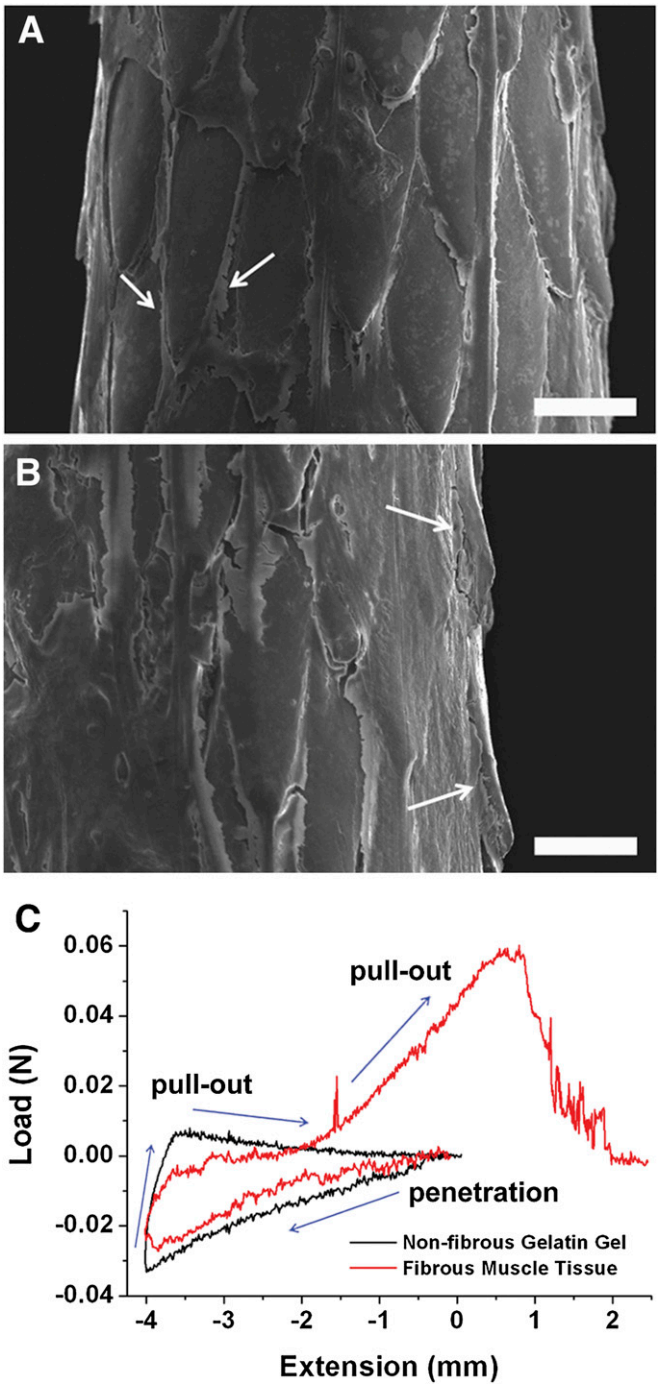

Fig. S6. Barbs mechanically interlock with tissue fibers during pull-out. (*A* and *B*) Characteristic FE-SEM images following removal of a barbed quill following a 4 mm penetration depth into tissue (For the FE-SEM image of the quill before penetration into tissue, see Fig. 1*B*). Residual tissue was present along the length of the barbs and under the barbs as indicated with white arrows. (Scale bar: 50 μm.) (*C*) Representative force-extension curves show penetration and pull-out forces that were obtained with fibrous muscle tissue and a density matched nonfibrous model tissue fabricated from gelatin gel (n = 5).